Refractive index sensor based on terahertz epsilon negative metamaterial absorber for cancerous cell detection

P. MUKHERJEE[1], S. BANERJEE[1], S. PAHADSINGH[1], W. BHOWMIK[1], B. APPASANI[1,*], Y. I. ABDULKARIM[2]
[1]*School of Electronics Engineering, Kalinga Institute of Industrial Technology, Bhubaneswar 751024, India*
[2]*Medical Physics Department, College of Medicals & Applied Science, Charmo University, 46023, Chamchamal, Sulaimania, Iraq*

The following paper proposes a novel design of a terahertz metamaterial absorber that can be used for refractive index sensing to detect cancerous cells. An epsilon negative metamaterial (ENG) with concentric octagonal ring resonators yields a near-perfect absorption rate of 99.19% at 3.076 THz. High values of the metrics like figure of merit (157.1 /RIU) and quality factor (307.1) indicate superior performance of the proposed design. The input parameters in the design are justified by parametric analysis. In addition, the absorption bands for different types of cells with distinctly different refractive indices are compared thus enabling the detection of cancerous cells.

(Received June 20, 2022; accepted April 5, 2023)

Keywords: Metamaterial absorber, Refractive index sensor, Terahertz, Cancer cell detection, Absorption, Sensitivity

1. Introduction

Cancerous basal cells [1] emerge in the form of skin cancer, mostly in adults, in which the number of clusters of cancerous cells increases rapidly, along with the size, in its advanced stage. Jurkat cells [2], a type of T-lymphocyte cells, are responsible for blood cancer in children. An increase in cancerous cell clusters results in spill-over of the cells into the bloodstream, thus spreading to other body organs. Hence, early efficient detection of such malignant cells is essential. This can be made possible by using periodic structures of sub-wavelength units [3] called metamaterials. When the incident light on these periodic units is converted into heat energy to evaluate the absorption rate, the structure is called a metamaterial absorber (MA). They are preferably designed using low-loss dielectrics atop a substrate made of photoconductive materials like GaAs [4], [5]. The peculiarity of periodic structures gives rise to negative refractive index [6] and backward propagating waves [7], properties otherwise not found in naturally occurring materials. Hence, several works emphasize adjusting the optical and electromagnetic characteristics made possible with such designs.

The tuneability of MAs is utilized in devising many sensing applications, such as temperature sensors [8], biomedical sensing [9,10] and imaging [11], etc. In this paper, a terahertz MA (TMA) is proposed to sense the refractive indices of the surrounding medium. In biomedical samples, the refractive index ranges from 1.3 to 1.39. In metamaterials, the excitation of surface plasmons in the metal-dielectric interface leads to the development of surface plasmon resonance (SPR). Apart from the construction of MMs, SPR has been established in [12] by coating MoS2 and Al metal atop a prism for imaging in the near-infrared (NIR) region. Multilayer dielectrics called photonic crystals can also be used to regulate SPR [13]. Other techniques for refractive index sensing include optical fiber sensing (OFS) and guided mode resonance (GMR) have been implemented throughout literatures [14] – [15]. In [15], a nano-cylindrical array of SiN4 and sodium, with SiO2 as the dielectric has been used as an RI sensor in the NIR region. The structure works under the principle of grated GMR over a refractive index range of 1.330 to 1.340 to obtain a sensitivity of 852 nm/RIU. Among these, SPR-based MMs have comparatively low cost. They implement label-free detection [16] for which only a small amount of sample is needed [12]. The technique is also beneficial because unlike other techniques, the samples do not need to be purified or filtered. In addition, they enable real-time monitoring [17] useful for practical biomedical implementations. The terahertz (THz) frequency range is preferred for various sensing applications since, in this range, measurements can be performed sans destruction due to non-ionizing radiation. A large bandwidth, low scattering and high penetration depth also ensure accurate sensing and imaging performance. An early demonstration of TMA sensing was presented by Cong et al. in 2014 [18]. A multi-band TMA for refractive index sensing is proposed for three distinct resonant frequencies with sensitivities of 0.540 THz/RIU, 0.7 THz/RIU, and 1.5 THz/RIU [19]. Du et al. [20] proposed graphene-based TMA for refractive sensing applications with a high sensitivity of 1.85 THz/RIU for a refractive index range 1.0-1.8. TMA-based biosensor essential for cancer detection is reported in [21], where a metamaterial absorber is designed with a polyimide substrate and gold metal patches, and a sensitivity of 1.649

THz/RIU is exhibited. RI sensing through SPR for the detection of cancerous cell has been proposed in [22]. For this purpose, a plasmonic metasurface was designed that yielded a sensitivity of 1250 nm/RIU for RI ranging from 1.6 – 1.9 with 0.2 step width. La Spada et al. Reference [23] used an MA for cancer detection in the GHz range and observed absorption shift in case of malignant behavior. Proper control of the EM properties of the TMA can also result in a high resolution [24] and appropriate absorbing frequency bandwidth. Reference [25] proposes a TMA using two Concentric Ring Resonators (CRRs) for cancerous cell detection. However, we find that the absorption peaks are furnished with higher bandwidth, and lower absorption as the refractive index of the surrounding medium gradually increases following a constant step size. In [26] ad [27], TMAs with low sensitivity of 0.2695 THz/RIU and 0.1392 THz/RIU have been proposed. Reference [28] also suggests a unique TMA using Split Ring Resonators (SRRs) for biomedical sensing, but it suffers from a very low magnitude of sensitivity. In [29], another TMA is proposed for biomedical sensing but with very limited sensitivity. Moreover, in [25][28][29], the designs also suffer from polarization angle variations as they are not at all polarization- insensitive, thereby reducing their practical feasibility. So, there is an absolute need to design a TMA that can detect the cancerous cells with high sensitivity and whose absorption characteristics do not change with the polarization angle alterations. Hence, this paper depicts a very simple yet unique design of a TMA which possesses polarization-independent characteristics and shows up high sensitivity of detecting cancerous cells, such as basal and jurkat. Table 1 further justifies the performance of the proposed TMA for the detection of cancerous cells in terms of Sensitivity, Quality Factor (Q-Factor), and Figure of Merit (FoM).

Table 1. Comparison of performance of the sensor

Refractive Index (*n*) Range	**Sensitivity**	**FoM (RIU^{-1})**	**Q-Factor**	**Reference**	**Biomedical Sensing**
1.36 – 1.4	1.65 THz/RIU	5.92	11.3	[21]	Yes
1.34 – 1.39	1.5 THz/RIU	25	44	[25]	Yes
1 – 1.5	0.2695 THz/RIU	5.39	48.3	[26]	Yes
1.4 – 2.0	0.1392 THz/RIU	3	15	[27]	No
1.1 – 1.9	187 GHz/RIU	6.015	32.167	[28]	Yes
1.0 – 1.39	0.3 THz/RIU	2.94	22.05	[29]	Yes
1.0 – 1.6	851 GHz/RIU	3.16	13.76	[30]	Yes
1 – 6	280 GHz/RIU	8.54	30.5	[31]	Yes
1.35 – 1.40	1.447 THz/RIU	36.175	92.75	[32]	Yes
1 – 1.6	3.923 THz/RIU	6.111	14.92	[33]	Yes
1.332, 1.372, 1.46, 1.76, 2.15	36.36 GHz/RIU	24	Not Reported	[34]	Yes
1 – 1.09	42.86 THz/RIU	19.44	475	[35]	No
1.35 – 1.39	1.571 THz/RIU	157.10	307.6	Proposed paper	Yes

The next section explains the structural design of the proposed model, followed by simulation results. Thereafter, the absorption mechanism and a parametric analysis are discussed in the third section. The fourth section presents the design's refractive index sensing capability, and in the last section, the conclusion is presented.

2. Experimental

This paper proposes a novel design for a metamaterial absorber useful in detecting cancer cells. Fig 1 shows the schematic diagram of our proposed design. The metal placed at the top and bottom of the structure is gold and gallium arsenide (GaAs, ε_r = 12.94, loss tangent $tan\delta$ = 0.006) with thickness h = 6 μm is the dielectric spacer [32]. The conductivity of gold is taken as 4.1 x 10^7 S/m [32]. The value of thickness h is sufficiently low to enhance THz design's mechanical flexibility. Gold is selected as the metal patch due to its reflective and low-loss properties. GaAs is a highly suitable semiconductor for high-frequency applications owing to its high electron mobility, and absorption and emission of light become efficient. Three concentric octagonal ring resonators, each of thickness t = 2 μm are placed on the GaAs substrate. The length of the unit cell, u = 100 μm, and, $r1$ = 45 μm, $r2$ = 40 μm, $r3$ = 35 μm, $r4$ = 30 μm, $r5$ = 25 μm, $r6$ = 20 μm. The ground metal

plane is such that the transmission of EM waves is sufficiently prevented. Along *x* and *y* axes, periodic boundary conditions are applied while transverse electromagnetic (TEM) wave excitation is received along the *z* axis. The design of the structure and all associated simulations are performed in CST Microwave Studio.

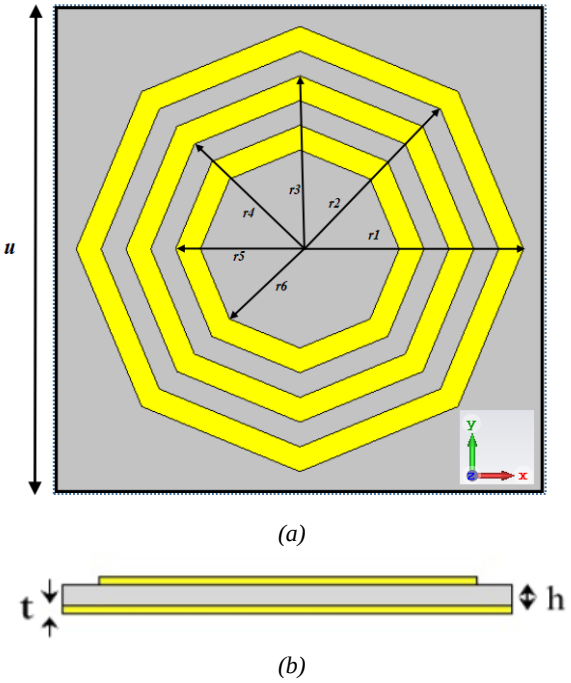

Fig. 1. The proposed design in (a) Top view and (b) Side view (color online)

3. Results and discussion

In order to determine the absorption of the structure, the reflection and transmission of the incident plane wave needs to be eliminated. For an efficient terahertz MA, the absorption is given by:

$$A = 1 - R - T = 1 - {S_{11}}^2 - {S_{21}}^2 \qquad (1)$$

where *A*, *R*, and *T* are the coefficients of absorption, reflection, and transmission, respectively. Since transmission of EM waves is prevented, $T = 0$. From Eq. 1, it can also be observed that the reflection coefficient should be negligible in order to maximize absorption. The detection of the cancerous cells depends on the analysis of the absorption spectrum of the proposed sensor, shown in Fig 2 (a). For the resultant peak, near-perfect absorption of 99.19 is observed at 3.076 THz, and the full-width half-maximum (FWHM) is determined to be 0.01 THz, thus showing a narrow absorption bandwidth required for sensing applications. Further, the Q-factor of the proposed design is calculated using equation (2), which comes out to be 307.6. It is a vital metric to justify the sensor's performance and a high value is always desired.

$$Q = \frac{f_0}{FWHM} \qquad (2)$$

where, f_0 is the resonant frequency. Since the structure is laterally symmetrical, it is polarization independent that ensures practical utility of the design. For ease in obtaining results, the structure is simulated at a polarization angle of 0°.

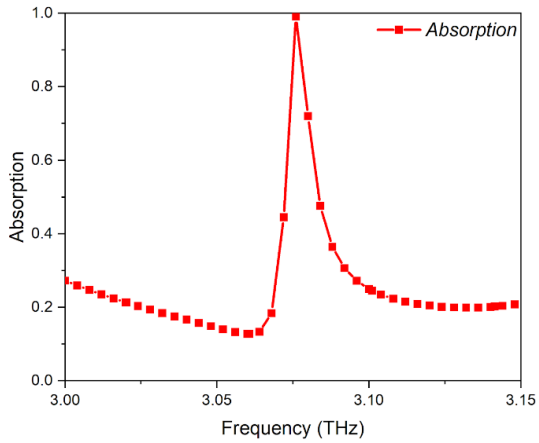

Fig. 2. Absorption characteristics of the TMA (color online)

The absorption characteristics obtained for hexagonal and circular rings is compared with that obtained for the octagonal rings used in the model. It can be observed from Fig. 3, that neither of the graphs presents a distinct high absorption. The graphs show an absorption band that is not practically feasible with very low absorption rates and higher bandwidth, hence justifying the choice to use the octagonal resonators instead of the circular and hexagonal ones. Increasing or decreasing the number of resonators, the absorption rate is still comparatively lesser (around 90%), qualifying the use of three octagonal resonators as the justified design.

Table 2. Comparison of absorption bands with different shapes of concentric resonators

Shape of concentric rings	Absorption (%)	Resonant Frequency (THz)	FWHM (THz)	Q factor
Hexagonal	80.3	3.08	0.022	140
Circular	89	3.084	0.015	205.6
Square	70.3	3.084	1.6	1.9275
Octagonal	99.19	3.076	0.01	307.6

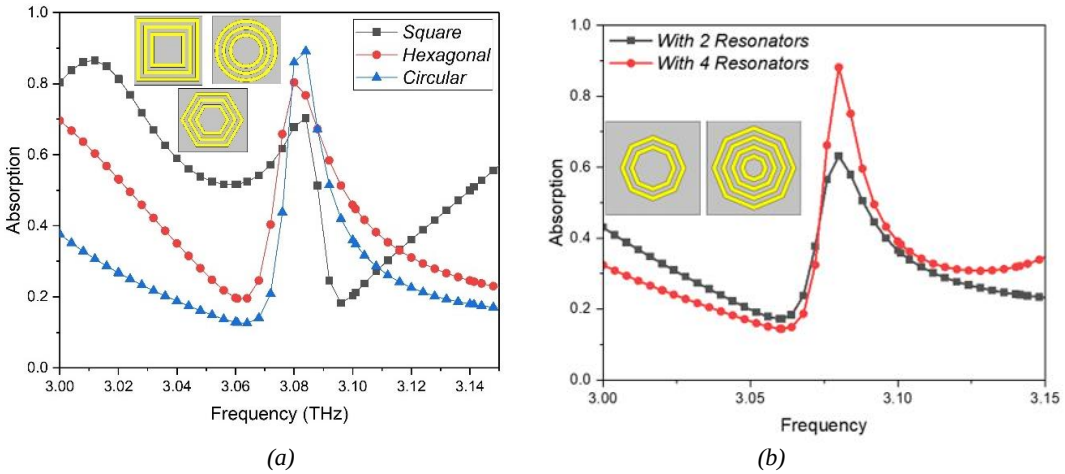

(a) *(b)*

Fig. 3. Variation in the (a) shape of the rings and (b) number of rings, with their corresponding absorption characteristics (color online)

The absorption of electromagnetic radiation is due to the matching of impedance to that of the free space. This can be understood from the input impedance (Z_{11}) plot shown in Fig. 4 (a). The input impedance at resonance frequency is 433.5 – *j* 69.1Ω, and its magnitude is 439Ω, which is close to the free space impedance of 377Ω. From Fig. 4(b), a negative permittivity and positive permeability is observed. The structure is thus an epsilon negative metamaterial (ENG) with a resonance that is plasmonic in nature. The input impedance, effective permeability and effective permittivity were obtained from the *s*-parameters using the following equations [36].

$$Z_{11}(f) = \sqrt{\frac{(1+S_{11}(f))^2 - S_{21}^2(f)}{(1-S_{11}(f))^2 - S_{21}^2(f)}} \tag{3}$$

$$\varepsilon_{eff}(f) = \frac{c}{j\pi f d}\left(\frac{1-S_{21}-S_{11}}{1+S_{21}+S_{11}}\right) \tag{4}$$

$$\mu_{eff}(f) = \frac{c}{j\pi f d}\left(\frac{1-S_{21}+S_{11}}{1+S_{21}-S_{11}}\right) \tag{5}$$

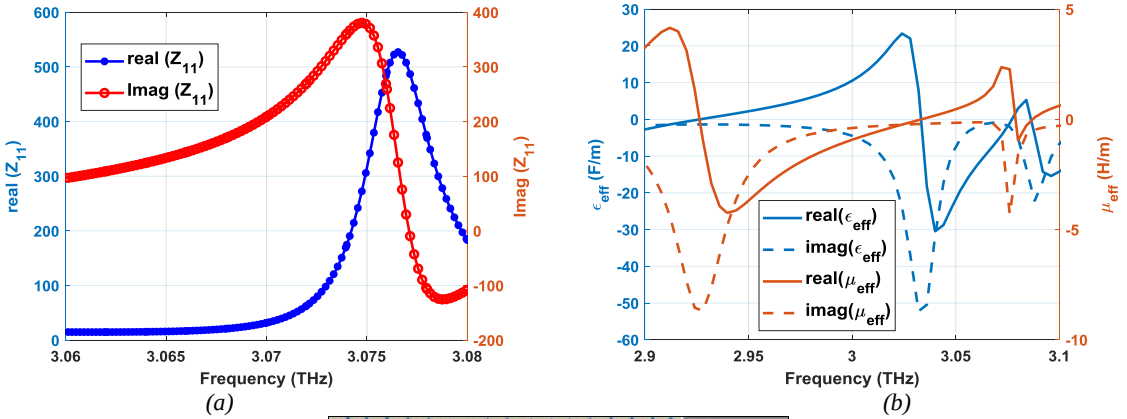

(a) *(b)*

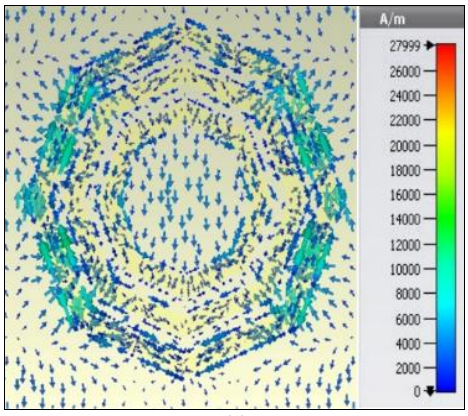

(c)

Fig. 4. Absorption mechanism (a) Input impedance (b) Effective permittivity and permeability (c) Surface current distribution (color online)

A detailed understanding of the absorption characteristics can be further inferred from the surface current distribution at the resonant frequency, given in Fig. 4 (c). The surface current is denser at the outer octagonal resonator than the inner resonators at the resonant frequency. A magnetic behavior is observed that, due to the presence of localized surface plasmon (LSPs) generates coupling. LSPs are charged oscillations present at the metal-dielectric interfaces. Magnetic coupling reduces the metallic absorption loss and leads to narrow absorption peaks at resonance. The current distribution along the top plane is also observed to move in an oscillating spiral, thus reducing density along with the inner concentric resonators. The current is weakly distributed at the top of the inner rings, while it is slightly larger along the edges. To justify the choice of parameters, a parametric sweep is performed for unit cell dimension, *u* and substrate height, *h*. Hence, an inverse relationship is observed between the parameter magnitude and the resonant frequency. Fig 5 (a) concludes that a unit cell dimension of u = 100µm provides the best absorption along with a narrow bandwidth, ultimately resulting in a better quality factor. From Fig 5 (b), it can be clearly observed that the optimal peak is obtained when the substrate thickness is h = 6 µm. A remarkable drop in the absorption rate is obtained by increasing or decreasing the substrate height. The absorption rate in a metamaterial absorber reaches its zenith when the impedance at input becomes equal to the impedance of the free space (approximately 377Ω). Hence, further changing the substrate height magnitude, this phenomenon of impedance matching is disrupted, and we observe a decrement in the absorption rate.

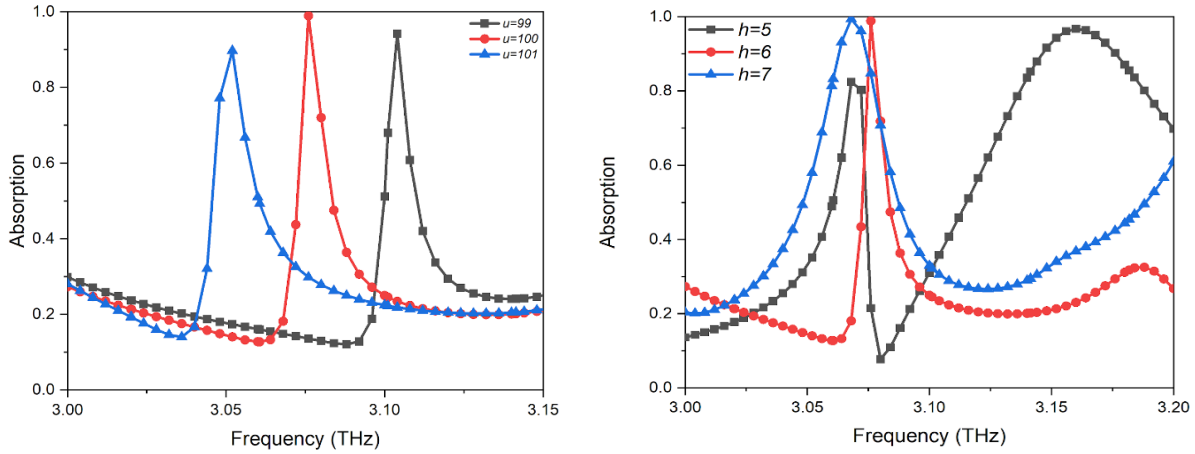

Fig. 5. Parametric sweep for (a) unit cell dimension and (b) height of the substrate (color online)

In designing an RI sensor, the materials must be so chosen that change in external temperature and pressure have negligible impact on their densities, and thus, the measurement of refractive index would not be interfered. In addition, it must also be insensitive to the polarization direction. By being insensitive to such external factors, the sensing applications prevent any and all forms of obstacles to attain optimum performance. Therefore, in sensing and imaging applications, refractive index sensors are widely preferred for biosensing applications like cancer detection, blood plasma detection, detection of analyte concentration, as gas sensors, as temperature sensors, etc.

The absorption spectra are obtained for different values of refractive index. This observation is important for effective cancer cells detection. In Fig. 6 (a), the absorption bands for refractive indices ranging from 1.35 to 1.39 are plotted with a step size of 0.01. Due to the very small variation in refractive index, the shift in the bands is significant, thus becoming highly sensitive to the refractive index in the surrounding medium.

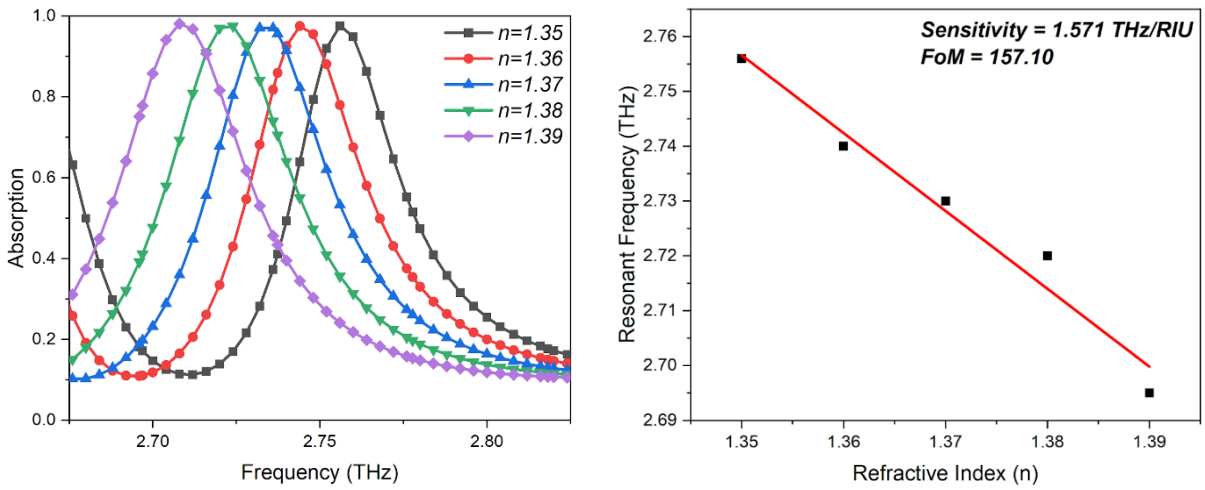

(a) *(b)*

Fig. 6. Absorption characteristics (a) for varying values of refractive index (b) Sensitivity (color online)

The sensitivity S, which is the ratio of the change in resonant frequency to that of the refractive index of the surrounding medium, and the corresponding FoM, which is the ratio of the sensitivity to the full-width half-maximum, i.e.,

$$FoM = \frac{S}{FWHM} \tag{6}$$

Hence by calculating the slope of the resonant frequency vs. refractive index plot in Fig. 6 (b), the sensitivity is found to be 1.571 THz/RIU, and FoM is 157.1. The resonant frequency can hence be expressed in terms of the refractive index as:

$$f = 4.87 - 1.571n \tag{7}$$

Fig. 7 shows the absorption spectrum for normal and cancerous Basal and Jurkat cells. Since cancer cells have abnormal cell cycles [37], the cancerous version of a particular cell type tends to have a higher refractive index value than its normal counterpart. As the value of the refractive index increases, the resonant frequency decreases.

Table 3. Absorption characteristics for normal and cancerous basal and jurkat cells

	Type of Cell			
	Basal		**Jurkat**	
	Normal	**Cancerous**	**Normal**	**Cancerous**
Refractive Index	1.36	1.38	1.375	1.39
Peak Absorption	94%	94.92%	94.81%	94.62%
Resonant Frequency	2.748	2.725	2.73	2.71
Q-Factor	61.06	68.125	56.875	54.2
FWHM	0.045	0.04	0.048	0.05

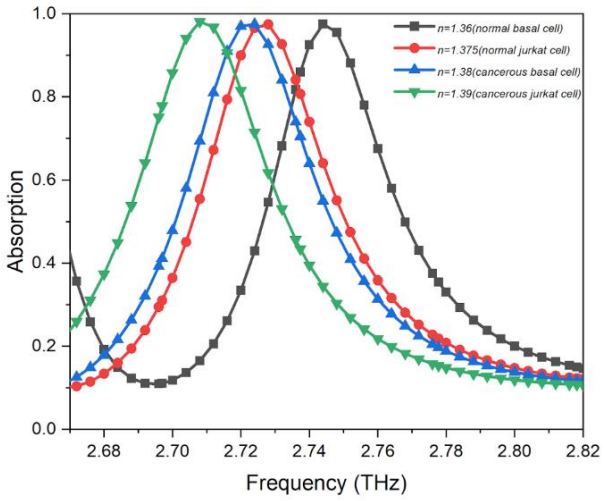

Fig. 7. Absorption characteristics for varying values of refractive index for normal and cancerous cells (color online)

4. Conclusion

The paper analyzes a novel design of a metamaterial absorber that can be used to detect cancer cells in the terahertz regime. This is brought into effect by modeling the absorber to become highly sensitive to changes in the refractive index in its surrounding medium. The proposed sensor thus acts as a refractive index sensing device with a sensitivity of 1.571 THz/RIU for refractive indices varying from 1.35 to 1.39. This sensor can be applied to any other biomedical samples with this range of refractive indices. However, we have focused only on cancer cells and obtained the absorption bands for the same. The efficacy of the design is also determined by a high Q-factor of 307.6 and an FoM of 157.10. It is attributed to its simple design, lightweight, and feasible use in biomedical sensing.

References

[1] S. Khakshour, T. V. Beischlag, C. Sparrey, Annual Int. Conf. IEEE Eng. Med. Biol. Soc., 6806 (2014).
[2] H. Piotrzkowska, J. Litniewski, A. Nowicki, E. Szymanska, IEEE Int. Ultrasonics Symp., 1 (2012).
[3] N. I. Landy, S. Sajuyigbe, J. J. Mock, D. R. Smith, W. J. Padilla, Phys. Rev. Lett. **100**(20), 207402 (2008).
[4] A. M. Buryakov, M. S. Ivanov, S. A. Nomoev, D. I. Khusyainov, E. D. Mishina, V. A. Khomchenko, I. S. Vasilevskii, A. N. Vinichenko, K. I. Kozlovskii, A. A. Chistyakov, J. A. Paixao, Mater. Res. Bull., **122**, 110688 (2020).
[5] A. L. Muñoz-Rosas, N. Qureshi, G. Paz-Martínez, C. G. Trevino-Palacios, J. C. Alonso-Huitron, A. Rodriguex-Gomez, Results in Physics **24**, 104095 (2021).
[6] D. R. Smith, J. B. Pendry, M. C. K. Wiltshire, Science **305**(5685), 788 (2004).
[7] V. G. Veselago, Soviet Physics Usp. **10**(4), 509 (1968).
[8] B. Appasani, Plasmonics **16**, 833 (2021).
[9] W. Wang, F. Yan, S. Tan, H. Li, X. Du, L. Zhang, Z. Bai, D. Cheng, H. Zhou, Y. Hou, Photon. Res. **8**, 519 (2020).
[10] S. K. Patel, J. Parmar, J. V. Sorathiya, T. K. Nguyen, V. Dhasarathan, Sci. Rep. **11**, 7101 (2021).
[11] N. I. Landy, C. M. Bingham, T. Tyler, N. Jokerst, D. R. Smith, W. J. Padilla, Phys. Rev. B **79**(12), 125104 (2009).
[12] Y. Xu, L. Wu, L. K. Ang, IEEE J. Sel. Top. Quant. Electron **25**(2), 1 (2019).
[13] Z. A. Zaky, A. M. Ahmed, A. S. Shalaby, A. H. Aly, Sci. Rep. **10**, 9736 (2020).
[14] J. Albert, L. Y. Shao, C. Caucheteur, Laser Photon. Rev. **7**(1), 83 (2013).
[15] Z. Huang, B. Wang, Surface and Interfaces **31**, 101987 (2022).
[16] I. Petrova, V. Konopsky, I. Nabiev, A. Sukhanova, Sci. Rep. **9**, 8745 (2019).
[17] D. Shankaran, K. Gobi, N. Miura, Sens. Actuators B Chem. **121**(1), 158 (2007).
[18] L. Cong, R. Singh, arXiv:1408.711 Physics Optics, (2014).
[19] S. Banerjee, P. Dutta, A. V. Jha, Progress in Electromagnetics Research **107**, 13 (2022).
[20] X. Du, F. Yan, W. Wang, L. Zhang, Z. Bai, H. Zhou, Y. Hou, Optics & Laser Technology **144**, 107409 (2021).
[21] Md. Azab, M. F. O. Hameed, A. Nasr, S. S. Obayya, IEEE Sensors Journal, **21**(6), 7748 (2021).
[22] M. R. Rakhshani, Photonics and Nanostructures-Fundamentals and Applications **43**, 100883 (2021).
[23] L. La Spada, F. Bilotti, L. Vegni, Proceedings of IEEE Sensors, 627 (2011).
[24] M. S. Heimbeck, H. O. Everitt, Adv. Opt. Photon. **12**, 1 (2020).
[25] S. Banerjee, U. Nath, P. Dutta, A. V. Jha, B. Appasani, N. Bizon, Inventions **6**(4), 78 (2021).

[26] S. Hu, D. Liu, H. Yang, Opt. Comm. **450**, 202 (2019).
[27] R. Yahiaoui, S. Tan, L. Cong, R. Singh, F. Yan, W. Zhang Journal of Applied Physics **118**(8), 083103 (2015).
[28] S. Banerjee, U. Nath, A. Shruti, 13th International Conference on Electronics, Computers and Artificial Intelligence (ECAI) 1 (2021).
[29] A. S. Saadeldin, M. F. O. Hameed, E. M. A. Elkaramany, S. S. A. Obayya, IEEE Sensors Journal **19**(18), 7993 (2019).
[30] M. R. Nickpay, M. Danaie, A. Shahzadi, Plasmonics **17**, 237 (2021).
[31] T. Chen, D. Zhang, F. Huang, Z. Li, F. Hu, Materials Research Express **7**(9), 095802 (2020)
[32] S. Banerjee, P. Dutta, A. V. Jha, B. Appasani, M. S. Khan, IEEE Sensors Letters **6**(6), 1 (2022)
[33] A. H. N. Razani, P. Rezaei, P. Zamzam, S. A. Khatami, O. M. Daraei, Optics Communications **524**, 128775 (2022)
[34] M. Askari, M. Bahadoran, Optik **253**, 168589 (2022).
[35] M. Askari, H. Pakarzadeh, F. Shokrgozar, Journal of the Optical Society of America B **38**(12), 3929 (2021).
[36] M. Askari, Z. Touhidinia, M. V. Hosseini, Journal of the Optical Society of America B **39**(4), 1282 (2022)
[37] R. K. Bista, S. Uttam, P. Wang, K. Staton, S. Choi, C. J. Bakkenist, D. J. Hartman, R. E. Brand, Y. Liu, Journal of Biomedical Optics **16**(7), 070503 (2011).

*Corresponding author: bhargav.appasanifet@kiit.ac.in